

## Plastic flow in polycrystal states in a binary mixture

Toshiyuki Hamanaka, Hayato Shiba, and Akira Onuki

*Department of Physics, Kyoto University, Kyoto 606-8502, Japan*

(Received 20 August 2007; revised manuscript received 7 January 2008; published 23 April 2008)

Using molecular dynamics simulation, we examine the dynamics of sheared polycrystal states in a binary mixture composed of small and large particles in two dimensions. We vary the composition  $c$  of the large particles and the shear rate  $\dot{\gamma}$  to realize changeovers among crystal, polycrystal, and glass. We find large stress fluctuations arising from sliding motions of the particles at the grain boundaries, which occur cooperatively to release the elastic energy stored. These stress fluctuations decrease as the system crosses over from polycrystal to glass. The dynamic processes are visualized with the aid of a sixfold angle  $\alpha_j(t)$  representing the local crystal orientation and a disorder variable  $D_j(t)$  representing a deviation from the hexagonal order for particle  $j$ .

DOI: [10.1103/PhysRevE.77.042501](https://doi.org/10.1103/PhysRevE.77.042501)

PACS number(s): 83.50.-v, 62.20.F-, 61.82.Rx, 61.43.-j

Understanding the deformation mechanisms of polycrystals under applied strain is of great scientific and technological importance in materials science [1–4]. If the typical grain size exceeds a critical size  $d_c \sim 10$  nm, the interplay of grain boundaries and dislocation motions determines the mechanical properties. For very small grain sizes less than  $d_c$ , some simulations suggested that plastic deformations are caused by sliding motions at the grain boundaries. However, these simulations are still fragmentary. In fact, a number of puzzles remain in polycrystal rheology, which have not yet been simulated microscopically, such as the Portevin–Le Chatelier effect in dilute alloys caused by intermittent yielding [5]. In physics, on the other hand, the dynamics of sheared glassy materials has been studied extensively [6,7], including microscopic particle systems [8–12], granular materials [13,14], and foams [15–17], while not enough attention has been paid to polycrystal rheology.

Recently, using molecular dynamics simulations, we have examined the dynamics of polycrystal states realized on very small scales in a model binary mixture in two dimensions [18]. The parameters we have changed are the size ratio of the diameters of the two components  $\sigma_2/\sigma_1$ , the temperature  $T$ , and the composition  $c$ . Polycrystal states appear as intermediate states between crystal and glass, where the grain boundary motions are severely slowed down in the presence of size dispersity  $\sigma_2/\sigma_1 \neq 1$ . As compared to the particles within the crystalline regions, those in the grain boundary regions are relatively mobile, giving rise to dynamic heterogeneity on long time scales. Namely, the origin of the dynamic heterogeneity is unambiguous in polycrystal states. We believe that investigating the jamming dynamics over wide ranges of  $\sigma_2/\sigma_1$  and  $c$  should help us to understand the glass dynamics, which still remains elusive, as the highly frustrated limit. In this paper, we will present simulation results on polycrystal rheology by changing  $c$  and the shear rate  $\dot{\gamma}$  at fixed  $\sigma_2/\sigma_1 = 1.4$ .

Our two-dimensional (2D) system is composed of the bulk region with volume  $V=L^2$  and the top and bottom boundary regions with volume  $0.1V$ , as can be seen in Figs. 1 and 2. Shear flow was realized by the relative boundary motion of the boundaries, where the top and bottom velocities are  $\pm \dot{\gamma}L/2$ . In the bulk region,  $0 < x, y < L$ , a mixture of

large and small particles interact via a truncated Lennard-Jones potential of the form  $v_{\alpha\beta}(r) = 4\epsilon[(\sigma_{\alpha\beta}/r)^{12} - (\sigma_{\alpha\beta}/r)^6] - C_{\alpha\beta}$ , where  $\alpha, \beta = 1, 2$ . It is characterized by the energy  $\epsilon$  and the soft-core diameter  $\sigma_{\alpha\beta} = (\sigma_\alpha + \sigma_\beta)/2$  with  $\sigma_2/\sigma_1 = 1.4$ . For  $r > r_{\text{cut}} = 3.2\sigma_1$ , we set  $v_{\alpha\beta}(r) = 0$  and the constant  $C_{\alpha\beta}$  ensures the continuity of  $v_{\alpha\beta}(r)$  at the cutoff  $r = r_{\text{cut}}$ . In this paper, we change the composition  $c = N_2/(N_1 + N_2)$  with  $N_1 + N_2 = 10^3$  in the bulk. The volume  $V$  is chosen such that the volume fraction of the soft-core regions is fixed at 1 or at  $\phi = (N_1\sigma_1^2 + N_2\sigma_2^2)/V = 1$ . For example,  $L = 33.1\sigma_1$  at  $c = 0.1$ . To each boundary ( $-0.1L < y < 0$  or  $L < y < 1.1L$ ), 100 small particles with radius  $\sigma_1$  are attached by the spring potential  $10\epsilon|r - \mathbf{R}_j|^2/\sigma_1^2$ . They also interact with the other particles in the boundary and bulk regions with the common Lennard-Jones potential. Before our simulation, the attached positions  $\mathbf{R}_j$  ( $j = 1, \dots, 100$ ) in each boundary wall were determined in

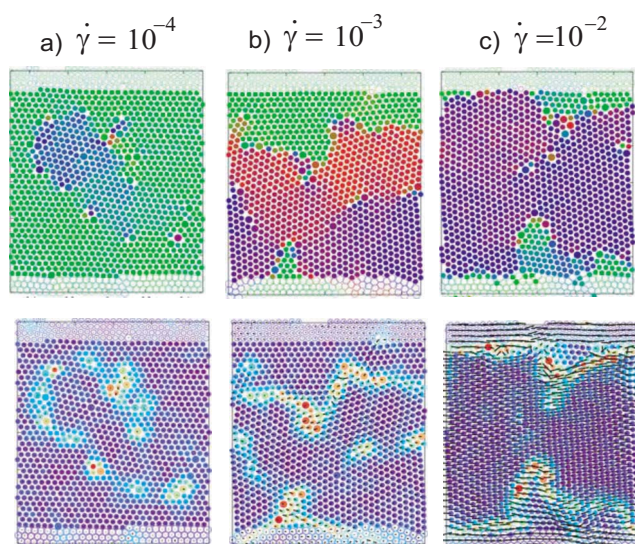


FIG. 1. (Color online) Sixfold orientation order (top) and disorder variable (bottom) for  $c=0.02$  in a binary mixture with  $\sigma_2/\sigma_1 = 1.4$ . Here  $\dot{\gamma} = 10^{-4}$  (left),  $10^{-3}$  (middle), and  $10^{-2}$  (right). The large particles form grain boundaries. Displacement vectors of the particles in a time interval of 10 (right) are also shown, which are large for  $\dot{\gamma} = 10^{-2}$ .

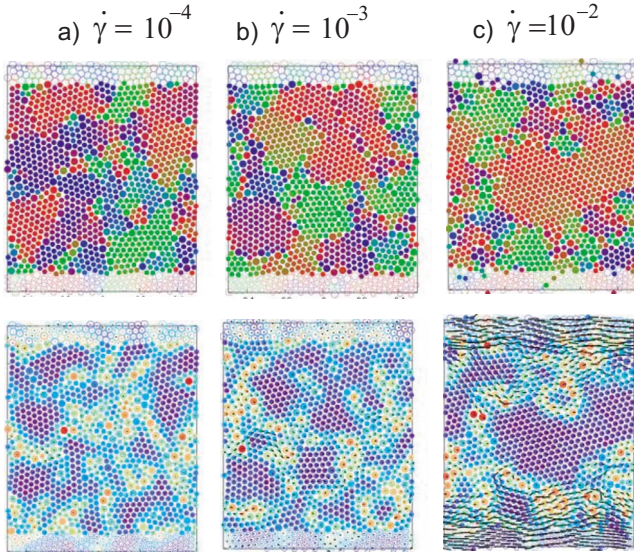


FIG. 2. (Color online) Sixfold orientation order (top) and disorder variable (bottom) for  $c=0.1$  for three shear rates as in Fig. 1. The grain structures for  $\dot{\gamma}=10^{-4}$  and  $10^{-3}$  are similar and are not affected by the boundaries, while the displacements are localized near the boundaries for  $\dot{\gamma}=10^{-2}$ .

a liquid state realized at  $T=2\epsilon/k_B$  with the Lenard-Jones potential only.

We integrated the Newton equations using the leapfrog algorithm [19] under the periodic boundary condition in the horizontal ( $y$ ) direction, with the mass ratio being  $m_1/m_2 = (\sigma_1/\sigma_2)^2$ . The time step of integration is  $0.002\tau$  with

$$\tau = \sigma_1 \sqrt{m_1/\epsilon}. \quad (1)$$

We will measure the time  $t$  in units of  $\tau$  and the shear rate  $\dot{\gamma}$  in units of  $\tau^{-1}$ . Without shear ( $\dot{\gamma}=0$ ), (i) we first equilibrated the system in a liquid state at  $T=2\epsilon/k_B$  in a time interval of  $10^3$  and then quenched it to the final temperature  $T=0.2\epsilon/k_B$ . (ii) After a relaxation time of  $5 \times 10^3$ , there was no appreciable time evolution in various quantities obtained as an average over the particles (see Fig. 7 of Ref. [18]). (iii) After these steps, we applied a constant shear to the system.

Since a large fraction of the particles are enclosed by six particles in 2D dense particle systems, the local crystalline order is represented by a sixfold orientation [20]. We define the orientation angle  $\alpha_j$  in the range  $[0, \pi/3]$  for each particle  $j$  using the complex number

$$\Psi_j = \sum_{k \in \text{bonded}} \exp[6i\theta_{jk}] = |\Psi_j| e^{6i\alpha_j}, \quad (2)$$

where the summation is over the particles “bonded” to the particle  $j$ . The two particles  $j \in \alpha$  and  $k \in \beta$  are bonded if their distance  $|\mathbf{r}_j - \mathbf{r}_k|$  is shorter than  $R_{\alpha\beta} = 1.25\sigma_{\alpha\beta}$  [9]. The upper cutoff  $R_{\alpha\beta}$  is slightly longer than the first peak position of the pair-correlation function  $g_{\alpha\beta}(r)$ . The  $\theta_{jk}$  is the angle of the relative vector  $\mathbf{r}_j - \mathbf{r}_k$  with respect to the  $x$  axis. Next we construct another nonnegative-definite variable representing the degree of disorder for each particle  $j$  by [18]

$$D_j = 2 \sum_{k \in \text{bonded}} [1 - \cos 6(\alpha_j - \alpha_k)]. \quad (3)$$

For a perfect crystal at low  $T$ , this quantity arises from the thermal vibrations and is nearly zero, but for particles around defects it assumes large values in the range 5–20.

At very small  $c$  and without shear, the large particles remain much separated in many cases in our simulation. Their long-distance diffusion is extremely slow at high densities. However, we can see a tendency for large particles with small separation to attract each other. If the system size is not too large, the particles form a single crystal in such quiescent states, where the defects (mostly created around the large particles) do not destroy the long-range crystalline order. However, with application of shear  $\dot{\gamma}$ , the large particles easily aggregate to form a grain boundary on the time scale of  $\dot{\gamma}^{-1}$ . In Fig. 1, we show such examples at  $c=0.02$ . The angles  $\alpha_j$  and the disorder variable  $D_j$  are displayed for  $\dot{\gamma}=10^{-4}$ ,  $10^{-3}$ , and  $10^{-2}$ . See Ref. [18] for the color map of  $\alpha_j$  and Fig. 4 below for that of  $D_j$ . At the largest shear  $\dot{\gamma}=10^{-2}$ , the large particles become more accumulated close to the boundaries. On the other hand, in one-component 2D crystals under large shear, high-density defects appear in slipping layers in shear-induced melting [21].

Next, Fig. 2 presents the results at  $c=0.1$ . Since the number of large particles is increased, their alignment along grain boundaries becomes more apparent, resulting in well-defined small-scale polycrystal grains. Remarkably, the grain structures are insensitive to  $\dot{\gamma}$  for not very large shear ( $\dot{\gamma} \lesssim 10^{-3}$  here), where the effect of the boundary walls does not extend into the bulk and the time average of the horizontal velocity is linear with the gradient being  $\dot{\gamma}$ . At this concentration, grain structures emerge even without shear [18], which closely resemble those in (a) and (b). To support this weakness of the boundary effect, almost the same grain structures were realized under the (periodic) Lee-Edwards boundary condition [19] (not shown in this paper). However, for very large shear  $\dot{\gamma}=10^{-2}$  in (c), the velocity gradient becomes localized near the boundaries, where larger crystalline regions are continuously rotated and deformed in the middle.

In Fig. 3, the shear stress  $\sigma_{xy}(t)$  is displayed in units of  $\epsilon\sigma_1^{-2}$  as a function of the average strain  $\dot{\gamma}t$  after application of shear at  $t=0$  for  $c=0.05$ ,  $0.1$ , and  $0.2$ , which is the sum of the microscopic shear-stress contributions over all the particles in the bulk divided by  $V$  [7,19]. For  $c=0.2$  the system is in a glass state. Each curve is a result of a single simulation run. Strong shear-thinning behavior can be seen in each panel. However, the results at the largest shear  $\dot{\gamma}=10^{-2}$  are affected by the boundary effect, as can be inferred from Figs. 1 and 2. The  $\sigma_{xy}(t)$  undergoes large temporal fluctuations, which obviously arise from intermittent plastic deformations of the grains. The level of fluctuations decreases with increasing  $c$ , because the typical grain sizes decrease with increasing  $c$ . Though the three curves are obtained for very different  $\dot{\gamma}$  in each panel, they behave similarly if plotted versus the strain  $\dot{\gamma}t$ . This means that the time scale of the intermittent yield is roughly proportional to  $\dot{\gamma}^{-1}$ . See the similar stress-strain curves calculated in glass in Refs. [11,12].

In Table I, we show the mean shear stress  $\langle \sigma_{xy} \rangle$  and the

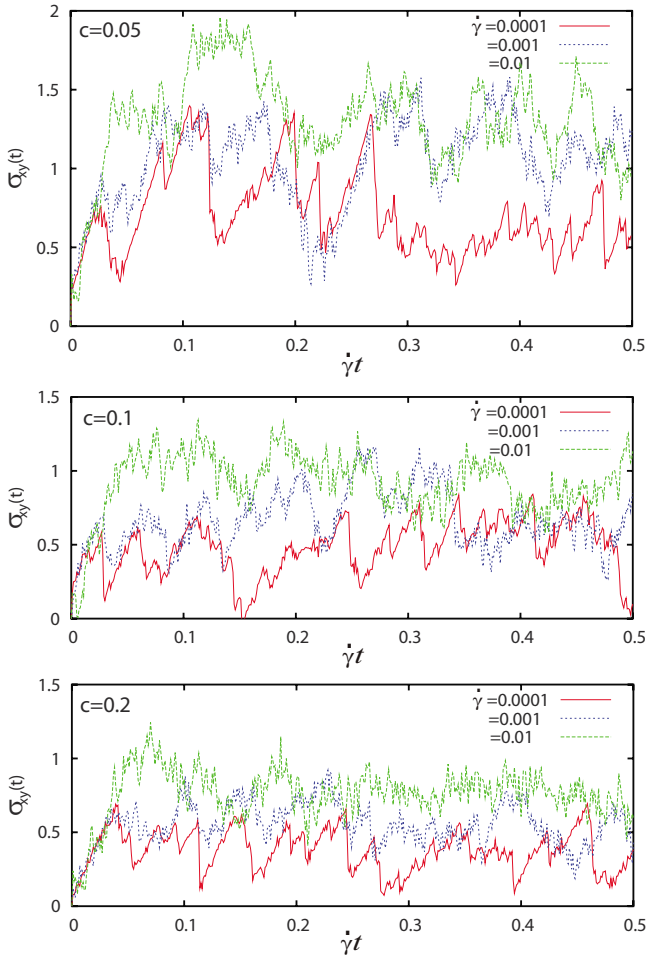


FIG. 3. (Color online) Shear stress  $\sigma_{xy}(t)$  vs strain  $\dot{\gamma}t$  after application of shear for  $c=0.05$  (top), 0.1 (middle) and 0.2 (bottom) in units of  $\epsilon\sigma_1^{-2}$ , where  $\dot{\gamma}=10^{-4}$ ,  $10^{-3}$ , and  $10^{-2}$  exhibiting strong shear thinning in each panel. Temporal fluctuations are weakened with increasing  $c$ .

variance  $\sqrt{\langle[\delta\sigma_{xy}]^2\rangle}$ , where  $\delta\sigma_{xy}(t)=\sigma_{xy}(t)-\langle\sigma_{xy}\rangle$  is the deviation and  $\langle\cdots\rangle=\int_{t_1}^{t_2}dt(\cdots)/(t_2-t_1)$  represents the time average between the two times  $t_1=0.2/\dot{\gamma}$  and  $t_2=0.5/\dot{\gamma}$ . Each set of mean and variance is the result of a single run, so the table

TABLE I. Mean shear stress  $\langle\sigma_{xy}\rangle$  (top) and square root of the time average of  $[\sigma_{xy}(t)-\langle\sigma_{xy}\rangle]^2$  (bottom) in the strain range  $0.2 < \dot{\gamma}t < 0.5$  for  $c=0.05, 0.1, 0.2,$  and  $0.3$  (in units of  $\epsilon\sigma_1^{-2}$ ) at shear rates  $\dot{\gamma}=10^{-4}$  (first line),  $10^{-3}$  (second line), and  $10^{-2}$  (third line).

Mean stress	$c=0.05$	$c=0.1$	$c=0.2$	$c=0.3$
$\dot{\gamma}=10^{-4}$	0.637	0.546	0.356	0.395
$\dot{\gamma}=10^{-3}$	1.07	0.717	0.548	0.581
$\dot{\gamma}=10^{-2}$	1.27	0.905	0.761	0.688
Variance	$c=0.05$	$c=0.1$	$c=0.2$	$c=0.3$
$\dot{\gamma}=10^{-4}$	0.199	0.157	0.135	0.155
$\dot{\gamma}=10^{-3}$	0.286	0.208	0.140	0.106
$\dot{\gamma}=10^{-2}$	0.191	0.141	0.099	0.144

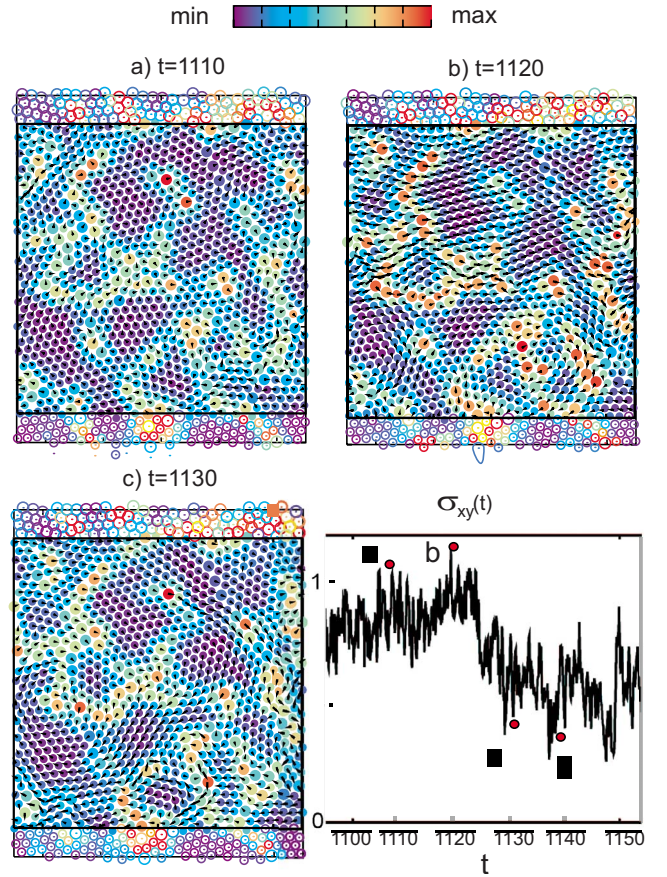


FIG. 4. (Color online) Disorder variable  $D_j$  at (a)  $t=1110$ , (b) 1120, and (c) 1130 at  $\dot{\gamma}=10^{-3}$ . The arrows represent the particle displacement  $\Delta r_j$  in the subsequent time interval of width 10, which is large in (b) for the particles in the grain boundary regions. The shear stress  $\sigma_{xy}(t)$  is also shown in this time region, which largely drops from  $b$  to  $c$ .

indicates only the trend in the rheology. In the table, these two quantities decrease with increasing  $c$  ( $\leq 0.2$ ), while they do not behave systematically at  $c=0.3$ . This should be due to the fact that the degree of disorder should be maximized between  $c=0.2$  and  $0.3$ . In polycrystal, we have  $\eta_{\text{eff}}=\langle\sigma_{xy}\rangle/\dot{\gamma}\sim\dot{\gamma}^{-a}$  with  $a=0.8-0.9$ . In glass, similar strong shear-thinning behavior with  $a\sim 1$  has been observed experimentally [22] and numerically [9].

In Fig. 4, we display  $D_j(t)$  at (a)  $t=1110$ , (b) 1120, and (c) 1130 at  $\dot{\gamma}=10^{-3}$ , superimposing the displacement vectors  $\Delta r_j(t)=r_j(t+\Delta t)-r_j(t)$  with  $\Delta t=10$ . The color is given to each picture independently, according to its minimum and maximum of  $D_j$ . See also the time evolution of  $\sigma_{xy}(t)$  in the corresponding time intervals,  $a-b$ ,  $b-c$ , and  $c-d$ . Between  $t=1110$  and 1120 ( $a-b$ ), as in picture (a), the deformations are mostly “elastic” and  $\sigma_{xy}(t)$  gradually increases with relatively small fluctuations. However, between  $t=1120$  and 1130 ( $b-c$ ), picture (b) demonstrates significant “sliding” particle motions in the grain boundary regions, which are of order  $\sigma_1$  even for this small  $\Delta t$ . These sliding motions are triggered collectively throughout the system (in our small system), leading to a catastrophic drop of  $\sigma_{xy}(t)$ . The particles written in orange, which are mostly larger ones, may

be regarded as being in disordered configurations. Their number is of order 10 in (a) and (c), while it is about 50 in (b). Between  $t=1120$  and  $1130$  (*c-d*), picture (c) indicates that noticeable particle displacements still continue. Large-scale collective motions within the grains are also conspicuous, which was already noticed in our previous simulation without shear [18].

In summary, in polycrystal states with very small grains, we have found intermittent yielding on a time scale of  $0.1 \dot{\gamma}^{-1}$  for not very large  $\dot{\gamma}$ . It is caused by cooperative sliding motions in the grain boundary regions in agreement with the atomistic simulations [1–4]. In our small-scale simulation, however, the yielding occurs coherently over the total system as in Fig. 4. Hence we cannot determine the spatial scale of the cooperative sliding extending over grains, which should be relevant in real systems. Further simulations of plastic deformations with much larger system sizes are thus informative. With increasing  $c$  ( $\leq 0.2$ ), the typical sizes of the crystalline regions become smaller and the stress fluctuations gradually decrease, as demonstrated in Figs. 1–3. That is, weaker disorder results in larger stress fluctuations in plastic

flow. The proportionality of the structural relaxation time to  $\dot{\gamma}^{-1}$  and the strong shear thinning behavior can be seen in polycrystal as in glass, as demonstrated in Fig. 3 and Table I.

In highly frustrated glasses, the spatial dimension of each shear-induced configurational change is limited [8,9,12], which should be distinguished from the coherent sliding in polycrystals. In glasses, such elementary events successively occur in their neighborhood eventually to form mesoscopic dynamic heterogeneity [8,9]. Also in the presence of shear, we should investigate the crossover from polycrystal to glass [18], which occurs rather abruptly in a narrow range of  $c$ . Such crossover effects could be investigated in colloidal mixtures on expanded space-time scales.

#### ACKNOWLEDGMENTS

This work was supported by Grants in Aid for Scientific Research and for the 21st Century COE project (Center for Diversity and Universality in Physics) from the Ministry of Education, Culture, Sports, Science and Technology of Japan.

- 
- [1] J. Schiotz, F. D. Di Tolla, and K. W. Jacobsen, *Nature (London)* **391**, 561 (1998).
- [2] A. Hasnaoui, H. Van Swygenhoven, and P. M. Derlet, *Phys. Rev. B* **66**, 184112 (2002).
- [3] S. Yip, *Nat. Mater.* **3**, 11 (2004).
- [4] V. Yamakov, D. Wolf, S. R. Phillpot, A. K. Mukherjee, and H. Gleiter, *Nat. Mater.* **3**, 43 (2004).
- [5] Y. Estrin and L. P. Kubin, *Mater. Sci. Eng., A* **137**, 125 (1991); G. D’Anna and F. Nori, *Phys. Rev. Lett.* **85**, 4096 (2000); P. Barat, A. Sarkar, P. Mukherjee, and S. K. Bandyopadhyay, *ibid.* **94**, 055502 (2005).
- [6] A. J. Liu and S. R. Nagel, *Nature (London)* **396**, 21 (1998).
- [7] A. Onuki, *Phase Transition Dynamics* (Cambridge University Press, Cambridge, England, 2002).
- [8] S. Kobayashi, K. K. Maeda, and S. Takeuchi, *Acta Metall.* **28**, 1641 (1980).
- [9] R. Yamamoto and A. Onuki, *J. Phys. Soc. Jpn.* **66**, 2545 (1997); R. Yamamoto and A. Onuki, *Phys. Rev. E* **58**, 3515 (1998).
- [10] M. Fuchs and M. E. Cates, *Phys. Rev. Lett.* **89**, 248304 (2002); K. Miyazaki and D. R. Reichman, *Phys. Rev. E* **66**, 050501(R) (2002).
- [11] F. Varnik, L. Bocquet, and J. L. Barrat, *J. Chem. Phys.* **120**, 2788 (2004).
- [12] C. E. Maloney and A. Lemaitre, *Phys. Rev. E* **74**, 016118 (2006).
- [13] B. Miller, C. O’Hern, and R. P. Behringer, *Phys. Rev. Lett.* **77**, 3110 (1996).
- [14] O. J. Schwarz, Y. Horie, and M. Shearer, *Phys. Rev. E* **57**, 2053 (1998).
- [15] T. Okuzono and K. Kawasaki, *Phys. Rev. E* **51**, 1246 (1995).
- [16] D. J. Durian, *Phys. Rev. E* **55**, 1739 (1997); S. A. Langer and A. J. Liu, *J. Phys. Chem. B* **101**, 8667 (1997).
- [17] P. Hébraud, F. Lequeux, J. P. Munch, and D. J. Pine, *Phys. Rev. Lett.* **78**, 4657 (1997).
- [18] T. Hamanaka and A. Onuki, *Phys. Rev. E* **74**, 011506 (2006); T. Hamanaka and A. Onuki, *ibid.* **75**, 041503 (2007).
- [19] J. P. Hansen and I. R. McDonald, *Theory of Simple Liquids* (Academic, London, 1986).
- [20] B. I. Halperin and D. R. Nelson, *Phys. Rev. Lett.* **41**, 121 (1978).
- [21] J. Delhommelle, *Phys. Rev. B* **69**, 144117 (2004).
- [22] J. H. Simmons, R. K. Mohr, and C. J. Montrose, *J. Appl. Phys.* **53**, 4075 (1982).